MATERIALS SCIENCE

Ultrastrong low-carbon nanosteel produced by heterostructure and interstitial mediated warm rolling

Bo Gao[1]*, Qingquan Lai[2]*, Yang Cao[1], Rong Hu[2], Lirong Xiao[1], Zhiyi Pan[1], Ningning Liang[1], Yusheng Li[1], Gang Sha[2], Manping Liu[3], Hao Zhou[1†], Xiaolei Wu[4,5†], Yuntian Zhu[1,6†]

Ultrastrong materials can notably help with improving the energy efficiency of transportation vehicles by reducing their weight. Grain refinement by severe plastic deformation is, so far, the most effective approach to produce bulk strong nanostructured metals, but its scaling up for industrial production has been a challenge. Here, we report an ultrastrong (2.15 GPa) low-carbon nanosteel processed by heterostructure and interstitial mediated warm rolling. The nanosteel consists of thin (~17.8 nm) lamellae, which was enabled by two unreported mechanisms: (i) improving deformation compatibility of dual-phase heterostructure by adjusting warm rolling temperature and (ii) segregating carbon atoms to lamellar boundaries to stabilize the nanolamellae. Defying our intuition, warm rolling produced finer lamellae than cold rolling, which demonstrates the potential and importance of tuning deformation compatibility of interstitial containing heterostructure for nanocrystallization. This previously unreported approach is applicable to most low-carbon, low-alloy steels for producing ultrahigh strength materials in industrial scale.

INTRODUCTION

Steels are the most widely used structural materials since the inception of the industrial age. Ultrastrong steels with low cost are highly desirable for large-scale industrial applications (1–3). Many approaches have been developed to make steels strong, among which increasing carbon content is, so far, most efficient and economical. However, increasing carbon content may lead to some undesired side effects such as degradation of weldability and workability (4, 5). Therefore, engineers and scientists have explored alternative approaches.

Recently, severe plastic deformation (SPD) techniques have been developed to produce ultrastrong nanostructured materials (6, 7). SPD techniques typically apply very large strains to refine the grain sizes of metals down to the ultrafine-grained regime (1000 to 100 nm) or even nanocrystalline regime (<100 nm) (8, 9). The major issues for using SPD techniques to produce ultrahigh strength materials include scaling-up and cost in industrial-scale productions (10). Nevertheless, the knowledge acquired from the SPD field can provide guidance for optimizing the microstructures and mechanical properties of steels.

Deformation-induced structural refinement is governed by the competition among dislocation generation, dynamic recovery, recrystallization, and grain boundary (GB) migration (11). Structural refinement is enhanced if the dislocation generation is enhanced or if dynamic recovery and recrystallization are suppressed during the deformation process. Dislocation generation is affected by both the external deformation mode and internal microstructure of materials. Microstructural heterogeneities are known to boost the densities of

both geometric necessary dislocations (GNDs) and statistically stored dislocations during plastic deformation (12). On the other hand, dynamic recovery and recrystallization annihilate dislocations, which impedes structural refinement. Lowering processing temperature or having precipitates in the material can slow down the kinetics of dynamic recovery and recrystallization but at the expense of deformability. In addition, the pinning effect of interstitial atoms on dislocations and interfaces help with achieving nanostructures. At moderate temperatures, the interstitial atoms are sufficiently mobile for dynamic segregation at dislocations. As a result, the mobility of dislocations and tendency for dislocation annihilation are reduced (13–15), which may cause the well-known dynamic strain aging phenomenon (15). Since the solute atoms act to pin dislocations, it will help with dislocation storage and consequently promote microstructure refinement.

In this work, we pursue the extreme structural refinement in a low-carbon steel by making use of the microstructural heterogeneities and interstitial atoms. A bulk ultrastrong (>2 GPa) low-carbon steel featuring nanolamellae with a record-breaking average thickness of ~17.8 nm was produced by simple industrial warm rolling at 300°C. Our experiments also show an unexpected observation that warm rolling may produce finer microstructures than cold rolling in the context of well-designed initial microstructures, which reveals a unreported principle of compatible codeformation in refining heterostructures by plastic deformation. Furthermore, this previously unreported strategy should be applicable to the majority of low-carbon and low-alloy steels and can be implemented in any steel mills without modification to existing facilities.

RESULTS

Cold rolling of the steel samples at room temperature for 30, 60, and 90% thickness reduction led to yield strengths of 1.01, 1.25, and 1.58 GPa, respectively (Fig. 1A). Unexpectedly, warm rolling of the same samples at 300°C for the same thickness reductions produced much higher yield strengths of 1.49, 1.73, and 2.05 GPa, respectively (Fig. 1B). These results contradict our conventional knowledge and intuition that cold rolling should produce higher strength because a lower

[1]Nano and Heterogeneous Materials Center, School of Materials Science and Engineering, Nanjing University of Science and Technology, Nanjing 210094, China. [2]Herbert Gleiter Institute of Nanoscience, Nanjing University of Science and Technology, Nanjing 210094, China. [3]School of Materials Science and Engineering, Jiangsu University, Zhenjiang 212013, China. [4]State Key Laboratory of Nonlinear Mechanics, Institute of Mechanics, Chinese Academy of Sciences, Beijing 100190, China. [5]School of Engineering Sciences, University of Chinese Academy of Sciences, Beijing 100049, China. [6]Department of Materials Science and Engineering, North Carolina State University, Raleigh, NC 27695, USA.
*The authors contributed equally to this work.
†Corresponding author. Email: hzhou511@njust.edu.cn (H.Z.); xlwu@imech.ac.cn (X.L.W.); ytzhu@ncsu.edu (Y.T.Z.)

temperature impedes the dislocation recovery and dynamic recrystallization. To explore the underlying physics of the higher strength obtained under warm rolling, microstructures of the steel samples are analyzed below.

The effect of rolling temperature on the microstructural evolution is demonstrated in Fig. 1 (A1 to A3 and B1 to B3). As shown in Fig. 1 (A1 to A3), cold rolling at room temperature led to gradual alignment of phase zones parallel to the rolling direction. However, the refinement of the martensitic phase was not very effective because the strong martensitic phase carried only a small fraction of the global plastic strain due to stain partitioning (16). With 90% of thickness reduction, some martensitic region in cold-rolled sample is still more than 2 μm in thickness, as shown in Fig. 1 (A3). In contrast, warm rolling at 300°C resulted in notable plastic flow in both the martensite and ferrite phases and even produced coshear bands at 60% thickness reduction (Fig. 1B2). After 90% rolling reduction, both the ferritic and martensitic zones were substantially refined and stretched along the rolling direction (Fig. 1B3).

Both the cold rolling and warm rolling produced nanolamellar structure (Fig. 2, A and B). However, at the same rolling, reduction of 90% warm rolling produced an average thickness of 17.8 ± 8.8 nm (Fig. 2, B and C), which is much thinner than what was produced by cold rolling (55 ± 25 nm; Fig. 2A). In the warm-rolled sample, nanolamellar structures are uniformly distributed (as shown in fig. S1). To our knowledge, this is a record fine structure among all dual-phase steels ever reported. The high-resolution transmission electron microscopy (TEM) image (Fig. 2D) shows the lattice structures in three distinct nanolamellae (labeled I, II, and III), which are separated by high-angle boundaries, as indicated by the fast fourier transformation (FFT) patterns (Fig. 2, E and F). While the lamella I is oriented to the $[0\overline{1}2]$ zone axis, the lamella II is at the $[\overline{1}11]$ zone axes. Therefore, the misorientation angle between lamellae I and II is 39°. The high-angle lamellar boundaries observed in Fig. 2 differ

from the reported low-angle boundaries in most SPD-processed single-phase metallic materials (17). The dislocation density within lamellae was measured to be as high as ~8.74×10^{16} m^{-2} (Fig. 2G). For the detail of dislocation density measurement, readers are referred to fig. S2.

Atom probe tomography (APT) analysis was conducted to reveal the distribution of alloying elements. Figure 3A shows that carbon atoms in the warm-rolled sample are agglomerated into planar features. On the other hand, distribution of Si and Mn atoms are uniform in the sample (Fig. 3B). It is noticed that even in the low-carbon content region, the weight fraction of carbon is still as high as ~0.1%, which is far beyond the carbon solubility in ferrite (18). Figure 3C reveals a clear fluctuation of carbon content with reference to the contents of Mn and Si, measured along the black line drawn in Fig. 3A. According to the carbon distribution in APT mapping, the measured average spacing between the carbon segregation peaks in the warm-rolled sample is ~15.2 nm, which is close to the lamellar thickness observed in TEM. Figure 3D shows that the strong segregation of carbon is usually constrained into a planar region with a width of ~3 nm. Analysis based on the APT result reveals that the planar regions with high-carbon content are actually the martensite lamellar boundaries, i.e., the ferrite-martensite interfaces. This key finding will be discussed later.

Figure 3 (E and F) shows that in the cold-rolled microstructure, a typical high carbon content region is of the size of ~50 nm, and Fig. 3 (G and H) shows that the average carbon content in this region is ~0.44%, which indicates that the region is martensite lamellae. Meanwhile, the weight fraction of carbon in the low-carbon content region is ~0.013%, which is close to ideal solubility of carbon in ferrite.

By comparing the distributions of carbon atoms in cold-rolled and warm-rolled steel samples (Fig. 3), it is indicated that interfaces served as diffusion pathways for carbon atoms from the prior martensite to the ferrite. The appropriate temperature during warm rolling
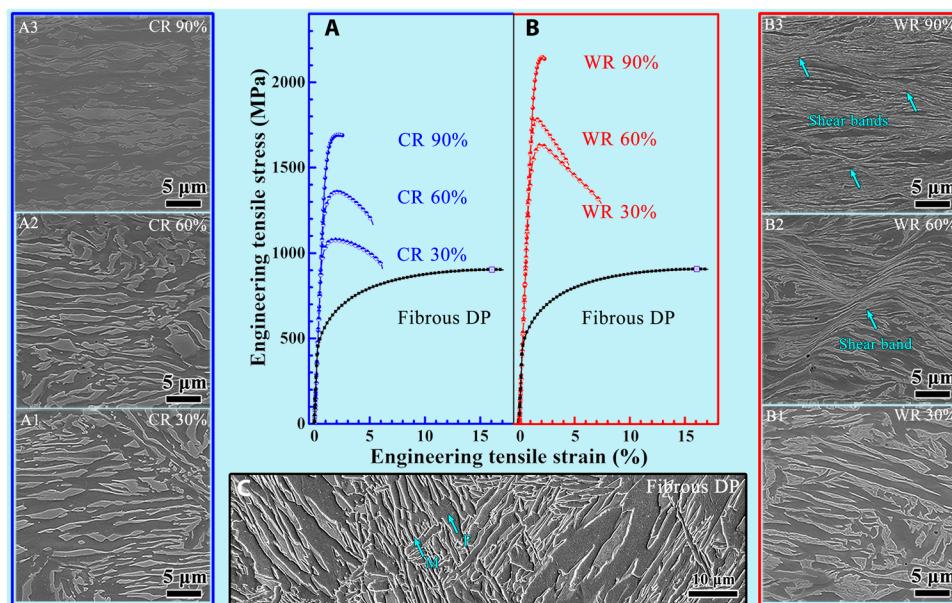

Fig. 1. Scanning electron microscopy micrographs and mechanical properties of typical steel samples. (**A** and **B**) Engineering stress-strain curves of the cold-rolled and warm-rolled steel samples as compared to the initial fibrous dual-phase (DP) samples. (A1), (A2), and (A3) are the scanning electron microscopy (SEM) micrographs showing the microstructures of the samples with cold rolling reduction of 30, 60, and 90%, respectively. (B1), (B2), and (B3) are the SEM micrographs the SEM micrographs showing the microstructures of the samples with warm rolling reductions of 30, 60, and 90%, respectively. (**C**) SEM micrograph showing the fibrous DP microstructure.
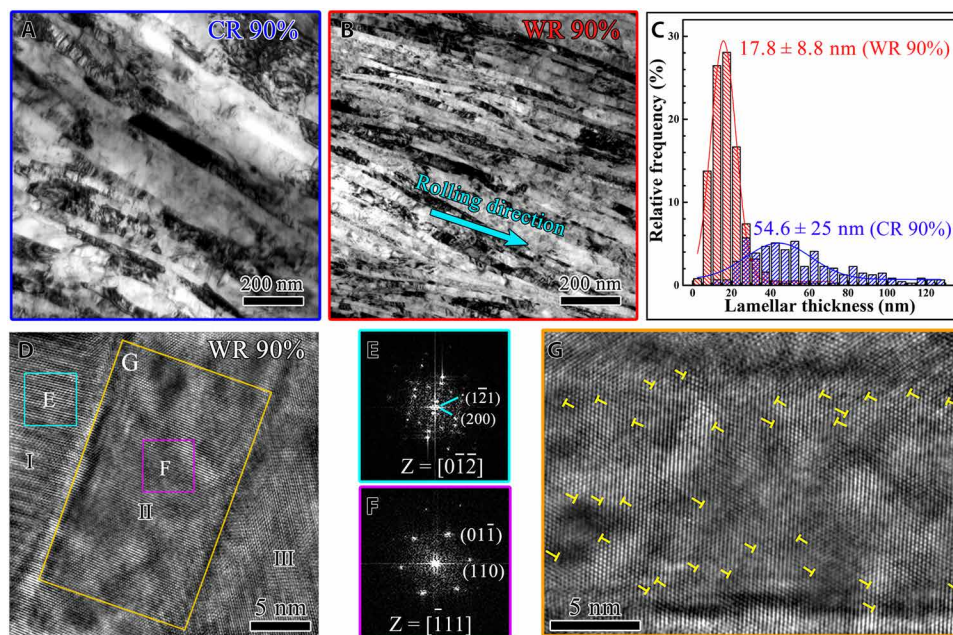
Fig. 2. TEM characterization of the as-rolled microstructures. (**A**) and (**B**) are bright-field TEM images showing the microstructures in the cold-rolled (CR) and warm-rolled (WR) steel samples, respectively. (**C**) The grain size distributions in rolled steel samples. (**D**) A high-resolution TEM image showing details in typical nanolamellae. Panels (**E**) and (**F**) are the diffraction patterns attained by fast fourier transformation in the selected areas in marked E and F in (D). (**G**) A high-resolution TEM image showing a high density of dislocations stored in a nanolamella.

is also important to enhance carbon segregation along martensite/ferrite interfaces.

It was expected that segregation of carbon atoms to nanolamellar interfaces helped with stabilizing the nanolamellae in the warm-rolled steels. Nanocrystalline structure usually becomes unstable upon heating and/or deformation (*19*). There are literatures showing that interfacial segregation and solute drag effect are capable of stabilizing the interfaces in alloys (*20, 21*). To verify this concept, in situ TEM observation was performed to analyze the thermal stability of the nanolamellae in the warm-rolled samples. Figure 4 (A to E) shows the evolution of the nanolamellar structures at the annealing temperature of 300°C for 0, 30, 60, 90, and 120 min, respectively. The thicknesses of the lamellar boundaries and the overall morphology in the area were nearly unchanged during annealing at 300°C (Fig. 4F), indicating that the nanolamellar structure was stable at this temperature. In situ heating experiments at the temperatures of 400° and 450°C were also performed. No growth of nanolamellae was observed until the annealing temperature was increased to 450°C (fig. S3). Systemic analysis on the microstructural and hardness results indicates that the thermal stability of the nanolamellae can be maintained at temperatures up to 400°C (fig. S4A).

It is worth noting that the warm rolling to 90% thickness reduction can make steel samples reach an ultimate tensile strength of 2.15 GPa, which is a record strength for low-carbon and low-alloy steels (Fig. 5A). Although steels with strengths above 2 GPa have been reported in the literature (*2, 3, 22*), they are associated with high-alloy contents that allow for the partitioning of alloying elements or the controlled precipitation to achieve a good mechanical performance, which not only increases the cost of raw materials and manufacturing processes(fig. S5) but also notably degrades their weldability (*4*). Figure 5B is a comparison between the strength of the warm-rolled steels

samples and those of steels with various carbon contents, highlighting the strengthening efficiency of extreme structural refinement as compared to that of carbon-adding approach. Therefore, from the perspective of manufacturing, warm rolling of heterostructured dual-phase steels is a previously unexplored, feasible, and economical approach for producing strong, low-cost steels in large-scale industrial manufacturing.

DISCUSSION
Heterostructures have been reported to produce heterodeformation-induced (HDI) hardening to improve ductility (*23*). In the as-rolled samples, the HDI hardening is not very effective due to two reasons: First, HDI hardening was caused by the piling up of GNDs. However, the nanothickness of the ferrite lamellae limits the GND pile up. The optimum lamellar thickness for HDI development has been found to be in the range of a few micrometers, as we observed earlier in Cu (*24*). Second, in the warm-rolled specimens, strength difference between the ferrite and martensite lamellae is markedly decreased, which reduces the HDI stress.

The advantage of the dual-phase heterostructure is its capability of sustaining large plastic strain. As a comparison, the full martensite of the same low-carbon steel can only be plastically deformed to 60% thickness reduction without fragmentation of the martensitic lamellae (fig. S6). In contrast, the dual phase structure is able to sustain 90% of reduction in both the cold and warm conditions, which is attributed to the good deformation compatibility in heterostructure. As demonstrated in the current study, it is unexpected that warm rolling produced much finer lamellar than cold rolling (Fig. 1), which contradicts our conventional intuition. This was caused by the improved mechanical compatibility and the higher plasticity of the martensite lamellae at the warm rolling temperature of 300°C. During
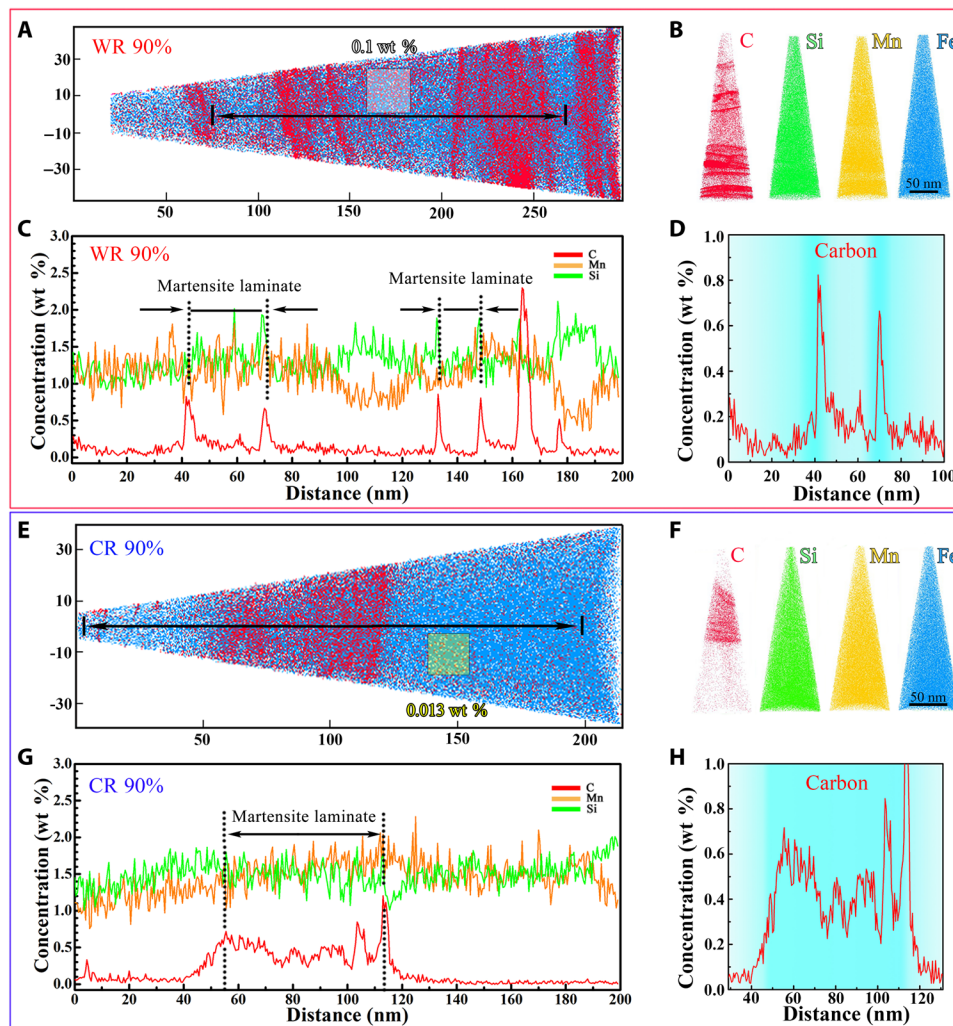
Fig. 3. APT analysis for the cold- and warm-rolled samples. (**A** and **B**) Three-dimensional (3D) atomic maps of C, Si, Mn, and Fe in a 90% warm-rolled sample. (**C**) Concentrations of C, Si, and Mn atoms measured along the black line drawn in (A). (**D**) Concentration of C atoms in range of 0 to 100 nm, referenced to (C). (**E** and **F**) 3D atomic mappings of C, Si, Mn, and Fe in a cold-rolled sample. (**G**) Concentration of C, Si, and Mn atoms measured along the black line drawn in (E). (**H**) Selected profile of C concentration in range of 30 to 130 nm, referenced to (G). wt %, weight %.

the cold rolling at room temperature, the martensite phase is much stronger than the ferrite phase, and ferritic lamellae will sustain most plastic strain. There is not enough stress that can be transferred to the martensitic lamellae to effectively deform them. At the same time, local stress concentrations will break the martensitic lamellae instead of uniformly deforming them, leading to the fragmentation of the martensitic lamellae (Fig. 1, A1 to A3). This conclusion is supported by the fact that full martensite of the same low-carbon steel can be plastically deformed to 60% thickness reduction without the fragmentation of martensitic lamellae (fig. S6). Therefore, heterostructures and the mechanical compatibility between the heterogeneous zones can be explored for effective structure refinement using plastic deformation.

Upon warm rolling, the codeformation of martensite and ferrite is enhanced (Fig. 1). This is due to the reduced mechanical incompatibility between the martensite and ferrite lamellae, i.e., reduced strength and increased plasticity in martensite at elevated temperatures (fig. S4B). The concept of codeformation has been explored in

the fabrication of multilayer metallic composite (e.g., Cu/Nb systems) or the production of UFG metals (e.g., ultrafine grained IF steels by accumulative roll bonding) (25–27). The current work finds that two constituent phases have the same crystal structure but of different carbon content and dislocation density. Different from the immiscible Cu/Nb system, the scale of microstructure during refinement cannot be stabilized by the phase boundary. Instead, the ferrite/martensite interfaces are stabilized by carbon segregation, which can only be observed at a moderate temperature. As a result, the warm rolling can produce much finer microstructure than ARB processing of IF steel (27).

At certain elevated temperatures (in the current case, ≤350°C), martensite laths were able to sustain large plastic strain before crack formation, and carbon atoms are diffused into the newly formed boundaries. According to the APT results in Fig. 3, redistribution of carbon atoms clearly occurred during warm rolling, and strong segregation of carbon atoms are found in the lamellar boundaries in the martensitic phase. Carbon segregation at interfaces helps with
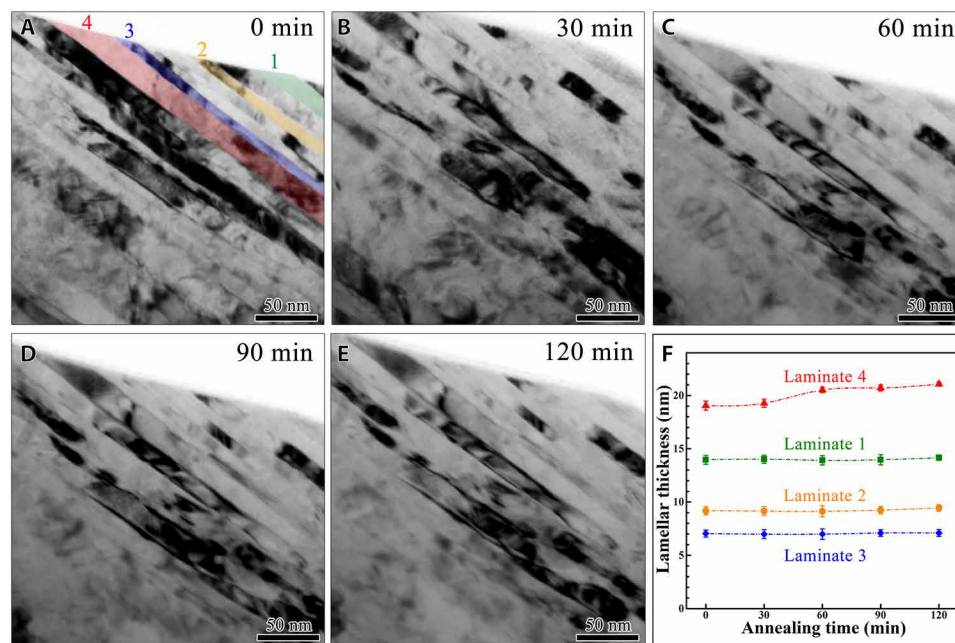
Fig. 4. In situ TEM observation of the microstructure stability at 300°C. (**A**) to (**E**) are the TEM images taken at the same location when the sample was maintained at 300°C for 0, 30, 60, 90, and 120 min, respectively. (**F**) Evolution of thicknesses of the numbered lamellae with respect to annealing time.
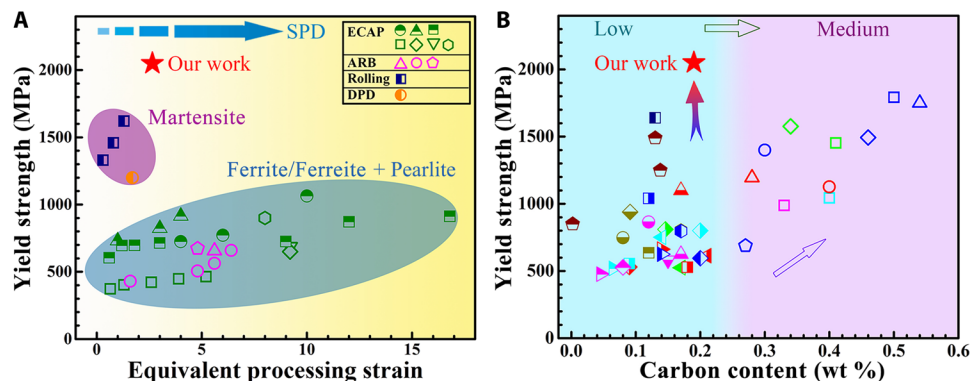

Fig. 5. Superior mechanical property. (**A**) A highlight of the efficiency of strengthening by warm rolling as compared to the results of other processing methods. (**B**) A highlight of the contribution of the extreme structural refinement to the strength of carbon steels. The relevant literatures for comparison are listed in table S1. ARB, accumulative roll bonding; DPD, dynamic plastic deformation; ECAP, equal channel angular pressing.

relaxing local stress and impedes GB migration (*28*), which is evidenced by the in situ TEM observation shown in Fig. 4. Solute segregation to dislocation boundaries and GBs notably lowers the migration kinetics of the boundaries and can thus help with stabilizing the nanostructures of the material (*7*, *29*–*31*). This idea has been widely adopted in designing stable nanocrystalline alloys (*32*, *33*). The enthalpy of segregation relative to the enthalpy of mixing determines the propensity for segregation. In this work, carbon segregation should have occurred during the grain refinement process due to the high diffusivity of interstitial carbon atoms and the high dislocation density produced by rolling. With increasing carbon segregation to the lamellar boundaries, the nanolamellae became more stable.

However, the warm-rolled nanolamellar structure may lose the thermal stability at temperatures higher than 350°C, as evidenced by the hardness drops (fig. S4A) and grain growth (fig. S3). Effect of

temperature on stability of interfacial segregation were well studied in previous works on formation of complexions by a simple annealing procedure (*34*). In this case, as the temperature increases to a certain high level, the driving force for GB migration increases notably, meanwhile the propensity for carbon segregation decreases at higher temperature, which reduces the overall pinning force on GBs (*35*, *36*).

In the warm-rolled sample, the ferritic phase becomes oversaturated with carbon atoms as indicated by the APT results in Fig. 3A. Oversaturation of carbon in ferrite can markedly strengthen ferritic phase, thus allowing ferrite to sustain a higher stress (*37*, *38*). The ferritic phase underwent extreme grain refinement, which enables it to sustain higher flow stress. The strength increases of the ferrite lamellae by both carbon oversaturation and grain refinement acted to reduce the mechanical incompatibility between the ferritic

and martensitic phases so that they can be codeformed to refine the microstructure.

The interstitial carbon atoms can also dynamically impede the motion of dislocations at moderate temperatures (13–15) and retard dislocation recovery. During plastic deformation of high purity metals, dislocations will quickly organize into the cell walls and subboundaries, creating dislocation cells and subgrains with dislocation-free interiors (7). In the present case, dislocations are organized to form the lamellar boundaries, but unexpectedly, high densities of dislocations also exist in the grain interiors (Fig. 2G). This is a strong indication of the carbon pining effect on dislocations. Therefore, diffusion of carbon atoms to ferrite is supposed to contribute substantially to the extreme grain refinement and increased dislocation storage in the ferritic phase.

It has been reported that the finest grain sizes of interstitial-free (IF) steel produced by accumulated rolling bonding and of the martensitic steel processed by cold rolling are ~210 (27) and ~200 nm (39), respectively. In contrast, by simple warm rolling, we produced nanolamellar structures with a mean boundary spacing of 17.8 nm in the heterostructured dual-phase steel. High-resolution TEM results show that the lamellar boundaries are high-angle GBs (HAGBs; Fig. 2, D to F). Unlike twinning, which changes the orientation of crystal structure to a fixed high angle, dislocation entanglement and accumulation tilt the crystal structure gradually (7, 9). Moreover, it has been noticed that lamellar boundaries created in metals are usually low-angle GBs even under SPD conditions (17). Without deformation twinning and further martensitic transformation, there should be other mechanisms active to help with the HAGB formation under the warm rolling condition. The misorientation of dislocation boundaries is determined by the arrangement of dislocations and their Burgers vectors (40). Dislocation arrangements near the interfaces of homogeneously structured and heterostructured materials are different. To accommodate the strain gradients in heterostructured materials, a large amount of GNDs with the same Burgers vector are formed, creating lattice bending and misorientation gradients (23), which should help with increasing the misorientation of the heterostructured interfaces, especially when these GNDs are absorbed by interfaces.

The key contributors to the ultrahigh strength observed in the warm-rolled low-carbon steel include the Hall-Petch strengthening of the prior soft ferrite by thin lamellar thickness, the dislocation strengthening by high intragranular dislocation density, and the solute strengthening by extra carbon solutes diffused from the martensitic region. In addition, the carbon segregation to the boundaries hinders the dislocation nucleation (31), and it has been reported that the plastic deformation in nanostructured metals is controlled by dislocation emission from GBs (9). As shown in fig. S7, the strength of IF steels generally follows the Hall-Petch relationship even down to ~20 nm, with the strengths of low-carbon steels slightly lying above those of IF steels, which indicates that the dominant strengthening contributor is lamellar thickness.

In conclusion, heterostructure-mediated warm rolling in conjunction with controlled solute diffusion and segregation offer a previously unexplored strategy for producing a bulk nanosteel with a record lamellar spacing of 17.8 nm, which has never been observed in single-phase martensite or ferrite to date. The nanosteel has a record-high yield strength of 2.05 GPa and ultimate strength of 2.15 GPa in the category of low-carbon steels. Our result leads to the conclusion that interstitial-containing heterostructure can be effectively explored to process stable nanolamellar structures by standard industrial processes. Reducing mechanical incompatibility among heterogenous domains is needed to effectively refine the heterostructure. The strategy reported here opens the door for large-scale manufacturing of low-carbon low-alloy steels with nanostructures and ultrahigh strength.

MATERIALS AND METHODS

The low-carbon steel used in this study has a nominal composition (weight %) of 0.19 C-1.01 Mn-1.46 Si. The processing of the nanol-amellar dual-phase steel can be divided into three sequential steps (fig. S9) The first step is to form a high density of lath martensite in the steel by austenitizing heat treatment at 950°C for 60 min and subsequent quenching in water. The second step is to obtain ultrafine fibrous ferrite-martensite dual-phase microstructure by intercritical annealing at 820°C for 10 min and subsequent quenching processes. The last step is to refine the microstructure of the low-carbon steel by rolling at designated temperatures. In searching for the rolling temperature for optimizing the mechanical properties of the steel sample in the current research, a series of rolling temperatures in the range between room temperature and 350°C was tested. For the warm rolling process, the dual-phase steel samples with a thickness of 8 mm and width of 30 mm were preheated at the designated temperatures for 20 min before rolling. The thickness reduction of each pass was ~0.5 mm, and the samples were reheated in the furnace for 5 min after each pass. Cold rolling was performed at room temperature with a thickness reduction of ~0.5 mm for each pass, and the sample was held in air for 2 min after each pass.

Microstructures were observed on the transverse plane using scanning electron microscopy and TEM. TEM was performed in a TECNAI 20 LaB6 G2 20 microscope operating at 200 kV. The TEM foils were ground down to ~20 μm in thickness and then thinned by ion milling at −30°C.

A local electrode atom probe (LEAP 4000X SI, Cameca Instruments) was used to analyze the element distributions in the cold- and warm-rolled samples. The measurements were performed in voltage mode at 50 K, and the pulse repetition rate was 200 kHz. Samples for APT analyses were prepared with the tips perpendicular to the rolling direction using a dual-beam focused ion beam (Zeiss Auriga).

Uniaxial tensile tests were performed at the strain rate of 3×10^{-3} s^{-1} on specimens with a gauge length of 10 mm and width of 2.5 mm. Five tests were repeated for each sample having the same microstructures.

SUPPLEMENTARY MATERIALS

REFERENCES AND NOTES

1. J. Zhao, Z. Jiang, Thermomechanical processing of advanced high strength steels. *Prog. Mater. Sci.* **94**, 174–242 (2018).
2. B. B. He, B. Hu, H. W. Yen, G. J. Cheng, Z. K. Wang, H. W. Luo, M. X. Huang, High dislocation density–induced large ductility in deformed and partitioned steels. *Science* **357**, 1029–1032 (2017).
3. R. Ding, Y. Yao, B. Sun, G. Liu, J. He, T. Li, X. Wan, Z. Dai, D. Ponge, D. Raabe, C. Zhang, A. Godfrey, G. Miyamoto, T. Furuhara, Z. Yang, S. van der Zwaag, H. Chen, Chemical boundary engineering: A new route toward lean, ultrastrong yet ductile steels. *Sci. Adv.* **6**, eaay1430 (2020).
4. O. S. Odebiyi, S. M. Adedayo, L. A. Tunji, M. O. Onuorah, F. Lambiase, A review of weldability of carbon steel in arc-based welding processes. *Cogent Eng.* **6**, 1609180 (2019).

5. Q. Lai, L. Brassart, O. Bouaziz, M. Gouné, M. Verdier, G. Parry, A. Perlade, Y. Bréchet, T. Pardoen, Influence of martensite volume fraction and hardness on the plastic behavior of dual-phase steels: Experiments and micromechanical modeling. *Int. J. Plasticity* **80**, 187–203 (2016).

6. Y. Estrin, A. Vinogradov, Extreme grain refinement by severe plastic deformation: A wealth of challenging science. *Acta Mater.* **61**, 782–817 (2013).

7. Y. Cao, S. Ni, X. Liao, M. Song, Y. Zhu, Structural evolutions of metallic materials processed by severe plastic deformation. *Mater. Sci. Eng. R* **133**, 1–59 (2018).

8. R. Z. Valiev, Y. Estrin, Z. Horita, T. G. Langdon, M. J. Zehetbauer, Y. T. Zhu, Fundamentals of superior properties in bulk nanoSPD materials. *Mater. Res. Lett.* **4**, 1–21 (2015).

9. Y. T. Zhu, X. Z. Liao, X. L. Wu, Deformation twinning in nanocrystalline materials. *Prog. Mater. Sci.* **57**, 1–62 (2012).

10. T. Müller, M. W. Kapp, A. Bachmaier, P. Felfer, R. Pippan, Ultrahigh-strength low carbon steel obtained from the martensitic state via high pressure torsion. *Acta Mater.* **166**, 168–177 (2019).

11. M. J. Starink, X. G. Qiao, J. Zhang, N. Gao, Predicting grain refinement by cold severe plastic deformation in alloys using volume averaged dislocation generation. *Acta Mater.* **57**, 5796–5811 (2009).

12. X. Wu, M. Yang, F. Yuan, G. Wu, Y. Wei, X. Huang, Y. Zhu, Heterogeneous lamella structure unites ultrafine-grain strength with coarse-grain ductility. *Proc. Natl. Acad. Sci. U.S.A.* **112**, 14501–14505 (2015).

13. Z. C. Luo, M. X. Huang, Revisit the role of deformation twins on the work-hardening behaviour of twinning-induced plasticity steels. *Scr. Mater.* **142**, 28–31 (2018).

14. A. S. Keh, Y. Nakada, W. C. Leslie, *Dislocation Dynamics* (McGraw Hill, 1968).

15. Y. Bergström, W. Roberts, The application of a dislocation model to dynamical strain ageing in α-iron containing interstitial atoms. *Acta Metall.* **19**, 815–823 (1971).

16. Q. Han, Y. Kang, P. D. Hodgson, N. Stanford, Quantitative measurement of strain partitioning and slip systems in a dual-phase steel. *Scr. Mater.* **69**, 13–16 (2013).

17. X. C. Liu, H. W. Zhang, K. Lu, Strain-induced ultrahard and ultrastable nanolaminated structure in nickel. *Science* **342**, 337–340 (2013).

18. H. Bhadeshia, R. Honeycombe, *Steels: Microstructure and Properties* (Butterworth Heinemann, 2017).

19. M. A. Meyers, A. Mishra, D. J. Benson, Mechanical properties of nanocrystalline materials. *Prog. Mater. Sci.* **51**, 427–556 (2006).

20. J. Hu, Y. N. Shi, X. Sauvage, G. Sha, K. Lu, Grain boundary stability governs hardening and softening in extremely fine nanograined metals. *Science* **355**, 1292–1296 (2017).

21. A. Devaraj, W. Wang, R. Vemuri, L. Kovarik, X. Jiang, M. Bowden, J. R. Trelewicz, S. Mathaudhu, A. Rohatgi, Grain boundary segregation and intermetallic precipitation in coarsening resistant nanocrystalline aluminum alloys. *Acta Mater.* **165**, 698–708 (2019).

22. S. Jiang, H. Wang, Y. Wu, X. Liu, H. Chen, M. Yao, B. Gault, D. Ponge, D. Raabe, A. Hirata, M. Chen, Y. D. Wang, Z. Lu, Ultrastrong steel via minimal lattice misfit and high-density nanoprecipitation. *Nature* **544**, 460–464 (2017).

23. Y. Zhu, X. Wu, Perspective on hetero-deformation induced (HDI) hardening and back stress. *Mater. Res. Lett.* **7**, 393–398 (2019).

24. C. X. Huang, Y. F. Wang, X. L. Ma, S. Yin, H. W. Höppel, M. Göken, X. L. Wu, H. J. Gao, Y. T. Zhu, Interface affected zone for optimal strength and ductility in heterogeneous laminate. *Mater. Today* **21**, 713–719 (2018).

25. T. Nizolek, I. J. Beyerlein, N. A. Mara, J. T. Avallone, T. M. Pollock, Tensile behavior and flow stress anisotropy of accumulative roll bonded Cu-Nb nanolaminates. *Appl. Phys. Lett.* **108**, 051903 (2016).

26. J. Chen, S. N. Mathaudhu, N. Thadhani, A. M. Dongare, Unraveling the role of interfaces on the spall failure of Cu/Ta multilayered systems. *Sci. Rep.* **10**, 208 (2020).

27. N. Kamikawa, T. Sakai, N. Tsuji, Effect of redundant shear strain on microstructure and texture evolution during accumulative roll-bonding in ultralow carbon IF steel. *Acta Mater.* **55**, 5873–5888 (2007).

28. R. Kirchheim, Grain coarsening inhibited by solute segregation. *Acta Mater.* **50**, 413–419 (2002).

29. Y. Lin, H. Wen, Y. Li, B. Wen, W. Liu, E. J. Lavernia, An analytical model for stress-induced grain growth in the presence of both second-phase particles and solute segregation at grain boundaries. *Acta Mater.* **82**, 304–315 (2015).

30. H. Zhou, G. M. Cheng, X. L. Ma, W. Z. Xu, S. N. Mathaudhu, Q. D. Wang, Y. T. Zhu, Effect of Ag on interfacial segregation in Mg–Gd–Y–(Ag)–Zr alloy. *Acta Mater.* **95**, 20–29 (2015).

31. Y. Li, D. Raabe, M. Herbig, P.-P. Choi, S. Goto, A. Kostka, H. Yarita, C. Borchers, R. Kirchheim, Segregation stabilizes nanocrystalline bulk steel with near theoretical strength. *Phys. Rev. Lett.* **113**, 106104 (2014).

32. H. A. Murdoch, C. A. Schuh, Stability of binary nanocrystalline alloys against grain growth and phase separation. *Acta Mater.* **61**, 2121–2132 (2013).

33. Y. J. Li, P. Choi, C. Borchers, S. Westerkamp, S. Goto, D. Raabe, R. Kirchheim, Atomic-scale mechanisms of deformation-induced cementite decomposition in pearlite. *Acta Mater.* **59**, 3965–3977 (2011).

34. M. Kuzmina, M. Herbig, D. Ponge, S. Sandlöbes, D. Raabe, Linear complexions: Confined chemical and structural states at dislocations. *Science* **349**, 1080–1083 (2015).

35. B. Schönfelder, G. Gottstein, L. S. Shvindlerman, Comparative study of grain-boundary migration and grain-boundary self-diffusion of [001] twist-grain boundaries in copper by atomistic simulations. *Acta Mater.* **53**, 1597–1609 (2005).

36. G. Gottstein, D. A. Molodov, L. S. Shvindlerman, Grain boundary migration in metals: Recent developments. *Interface. Sci.* **6**, 7–22 (1998).

37. Q. Han, A. Asgari, P. D. Hodgson, N. Stanford, Strain partitioning in dual-phase steels containing tempered martensite. *Mater. Sci. Eng. A* **611**, 90–99 (2014).

38. C. C. Tasan, M. Diehl, D. Yan, C. Zambaldi, P. Shanthraj, F. Roters, D. Raabe, Integrated experimental–simulation analysis of stress and strain partitioning in multiphase alloys. *Acta Mater.* **81**, 386–400 (2014).

39. X. Huang, S. Morito, N. Hansen, T. Maki, Ultrafine structure and high strength in cold-rolled martensite. *Metall. Mater. Trans. A* **43**, 3517–3531 (2012).

40. X. Liu, J. Wang, Low-energy, mobile grain boundaries in magnesium. *Sci. Rep.* **6**, 21393 (2016).